POLITECNICO DI TORINO
Repository ISTITUZIONALE

Interpretation of boundary conditions in the analytical and numerical shell solutions for mode analysis of multilayered structures

Original
Interpretation of boundary conditions in the analytical and numerical shell solutions for mode analysis of multilayered structures / Brischetto, S., Tornabene, F., Fantuzzi, N., Bacciocchi, M.. - In: INTERNATIONAL JOURNAL OF MECHANICAL SCIENCES. - ISSN 0020-7403. - 122:(2017), pp. 18-28. [10.1016/j.ijmecsci.2016.12.017]

Availability:
This version is available at: 11583/2661809 since: 2020-06-04T00:22:56Z

Publisher:
Elsevier

Published
DOI:10.1016/j.ijmecsci.2016.12.017

Terms of use:

This article is made available under terms and conditions as specified in the corresponding bibliographic description in the repository

Publisher copyright

(Article begins on next page)

16 October 2026

Interpretation of boundary conditions in the analytical and numerical shell solutions for mode analysis of multilayered structures

S. Brischetto‡*, F. Tornabene†, N. Fantuzzi† and M. Bacciocchi†

‡ Department of Mechanical and Aerospace Engineering, Politecnico di Torino, Torino, Italy

† DICAM Department, University of Bologna, Bologna, Italy

Abstract

The paper proposes the first 18 vibration modes for plates, and the first 14 vibration modes for cylinders and cylindrical shells. All the edges of these structures are simply supported and the free frequencies are calculated using an exact three-dimensional shell model. A comparison is proposed using two different numerical models such as a classical two-dimensional finite element model and a refined two-dimensional generalized differential quadrature model. The 3D exact model gives all types of vibration modes, when the four edges are simply supported, changing the imposed half-wave numbers m and n in the two in-plane directions α and β. Some of these modes have one of the two half-wave numbers equals zero. When this condition is simultaneously combined with the condition of transverse displacement different from zero, the resulting vibration mode is defined as cylindrical bending mode. The cylindrical bending case has all the derivatives made in the direction where $m = 0$ or $n = 0$ equal zero. This feature means that the vibrational behavior does not change along this particular direction. The numerical models with the simply supported boundary conditions for all the edges do not achieve these results. These cylindrical bending numerical results are obtained modifying the boundary conditions. Proposed results will demonstrate the validity of this idea and how to modify the mathematical models in order to obtain and improve the cylindrical bending solutions.

Keywords: 3D exact shell model; 2D finite element model; 2D generalized differential quadrature model; vibration modes; cylindrical bending; simply supported edges; free edges; boundary conditions.

1 Introduction

A comparison in terms of free frequencies between classical two-dimensional (2D) finite elements (FEs), classical and refined 2D generalized differential quadrature (GDQ) models and an exact three-dimensional method has been proposed by authors in [1] and [2] for single-layered and multilayered isotropic, composite and sandwich structures, and in [3] and [4] for single-layered and sandwich functionally graded structures. The proposed analyses considered plates, cylinders, and cylindrical and spherical panels. Low and high order frequency values were investigated for simply supported thick and thin structures. Vibration mode investigation was fundamental to understand how to compare

*Author for Correspondence: Salvatore Brischetto, Department of Mechanical and Aerospace Engineering, Politecnico di Torino, corso Duca degli Abruzzi 24, 10129 Torino, ITALY. tel: +39.011.090.6813, fax: +39.011.090.6899, e.mail: salvatore.brischetto@polito.it.

results obtained using the FE and GDQ solutions (numerical methods) and those obtained using the exact three-dimensional model. The 3D exact model calculates infinite vibration modes for each possible combination of half-wave numbers (m, n). A 2D numerical solution calculates a finite number of vibration modes, in fact it has a finite number of degrees of freedom considering the three directions α, β and z. A possible procedure to compare a 3D exact model with a 2D numerical model is the calculation of the frequency values via the 2D numerical code and then the evaluation of the 3D exact frequency values using the opportune half-wave numbers (obtained using the graphical visualization of the vibration modes by means of the GDQ or FE method). It is clear how the 3D model could give some frequencies that are not calculated by the 2D numerical models, but these considerations were not the aim of the past authors' papers [1]- [4]. Those works tried to explain what could be the advantages and the limitations of 2D numerical codes but they did not explain how to obtain the frequencies missed by the numerical methods.

The analysis proposed in the present paper tries to fill this gap calculating all the possible first 18 (for plates) or 14 (for shells) 3D exact frequencies for isotropic and orthotropic single- and multi-layered structures combining the half-wave numbers along the two directions α and β in the plane. 18 frequencies are calculated for the plate because some modes are twice given for material and geometrical symmetry reasons. In these first frequencies there are some modes that cannot be calculated by the 2D numerical models if structures are considered with four simply-supported edges. In general, these modes are those corresponding to the cylindrical bending condition which, in the 3D exact solution, means that one of the two half-wave numbers is equal to zero simultaneously with a transverse displacement different from zero along the edge where the half-wave number is different from zero. These results are not solutions of the 2D numerical models with the four simply supported edges, and it is necessary to build a different mathematical model where two edges are simply supported and the other two ones are free. In this way, cylindrical bending with the transverse displacement different from zero is allowed in numerical models. In this paper, the mathematical model which represents the numerical solution is opportunely modified changing the boundary conditions in order to obtain the missed frequencies and modes. This feature is possible only when the zero half-wave number is imposed through a rectilinear side because the half-wave number equals zero in the curvilinear edge does not mean that all the quantities in that direction are constant. This feature is due to the curvature presence. The new contribution of the present work is the investigation of cylindrical bending frequencies which can be obtained by 2D numerical models only modifying the boundary conditions. Such a comparison has never been made in past authors' works [1]- [4].

The cylindrical bending analysis is very common in the literature because its simplicity allows an immediate verification of the proposed structural models. Some plate models verified by means of cylindrical bending hypotheses were proposed in [5] where the responses of a simply supported cross-ply laminate in cylindrical bending with viscous interfaces were studied using the state-space method. The state-space method was also used in [6] and [7] for the investigation of simply supported angle-ply laminates with interfacial damage and for static load application to simply supported angle-ply laminated plates, respectively. Gandhi and Raval [8] proposed an experimental three-roller cylindrical bending for plates which was compared with analytical solutions. A methodology for the design of plate-forming dies in cylindrical bending, using optimization techniques to reduce the cost of die production, was discussed in [9]. As demonstrated in [10] for the large deflection of a thin beam, the solution of the plate problem is not unique under certain conditions. In [11], the cylindrical bending of laminates was analyzed using the bending-gradient plate theory as an extension of the Reissner-Mindlin plate model. The Reissner-Mindlin plate theory was also used in [12] for the cylindrical bending of elastic and composite plates subjected to the mechanical transverse loading response under plain strain conditions. Another recent publication regarding cylindrical bending conditions was presented in the work by Sayyad and Ghugal [13] where they investigated flat laminated plates using a nth order shear deformation theory. Well-known three-dimensional exact elasticity solutions for composite laminated

plates were developed by Pagano [14], [15], and then verified using the cylindrical bending conditions. A two-dimensional layer-wise model was introduced in [16] as an accurate and effective alternative to the finite element method. This model was extended to the analysis of delamination growth in multi-layered plates subjected to cylindrical bending loading. A new stress analysis method for the accurate determination of the stress distributions in angle-ply laminated plates subjected to cylindrical bending was proposed in [17]. Further cylindrical bending analyses for plates, which include functionally graded layers, can be found in [18] and [19]. The works [20]- [25] proposed the cylindrical bending analysis of flat plates embedding piezoelectric layers which can also be, in some cases, functionally graded in the thickness direction. The thermal loads in cylindrical bending for flat plates were considered in [26]- [28] where composite and/or piezoelectric layers were included. Other related papers about cylindrical bending for shell structures are not so numerous in the literature. The most important cases concern the cylindrical shells where the cylindrical bending conditions can be verified through the rectilinear edges. Chen and Lee [29] used the state-space formulation for the bending and free vibration analysis of simply-supported angle-ply laminated cylindrical panels in cylindrical bending. Wu and Syu [30] proposed a three-dimensional (3D) piezoelectric model for cylindrical shells under cylindrical bending electromechanical loads using the method of perturbation. The behavior of a simply supported angle-ply laminated cylindrical shell in cylindrical bending with viscoelastic interfaces was studied in [31]. Further interesting works can be found in [32]- [35] where dynamic analyses of cylindrical shells are proposed.

The present paper aims to compare the free frequencies obtained using a 3D exact shell model, a 2D classical finite element model and a 2D refined generalized differential quadrature model. The 3D exact shell model is based on the equilibrium equations written for the generic curvilinear orthogonal coordinates, they are solved in closed form imposing simply supported boundary conditions. The differential equations along z are solved using the exponential matrix method and the layer wise approach. Such model is detailed and validated in Section 2. The 2D FE and GDQ models are described in Section 3. The validation of these numerical approaches is also proposed in the same section. The 2D FE model is based on a well-known commercial finite element code. The 2D GDQ model has been implemented in an in-house academic software. The comparisons between these three different procedures are proposed in Section 4 and the main conclusions are remarked in Section 5.

2 3D exact shell model

The three-dimensional exact shell model used in Section 4 has been developed in [36]- [44] for several applications such as one-layered and multilayered isotropic, orthotropic, composite and sandwich structures, functionally graded structures, single- and double-walled carbon nanotubes. The equilibrium equations are written in a general orthogonal curvilinear coordinate system (α, β, z) valid for plates and shells with constant radii of curvature. These equations are solved in exact form supposing simply supported edges and using the exponential matrix method to solve the differential equations in z.

The three differential equations of equilibrium developed for the free vibration analysis of multilayered spherical shells (a particular case of doubly-curved shells with constant radii of curvature $R_\alpha = R_\beta$)

embedding N_{L} layers are:

$$H_\beta \frac{\partial \sigma^k_{\alpha\alpha}}{\partial \alpha} + H_\alpha \frac{\partial \sigma^k_{\alpha\beta}}{\partial \beta} + H_\alpha H_\beta \frac{\partial \sigma^k_{\alpha z}}{\partial z} + \left(\frac{2H_\beta}{R_\alpha} + \frac{H_\alpha}{R_\beta} \right) \sigma^k_{\alpha z} = \rho^k H_\alpha H_\beta \ddot{u}^k \ , \tag{1}$$

$$H_\beta \frac{\partial \sigma^k_{\alpha\beta}}{\partial \alpha} + H_\alpha \frac{\partial \sigma^k_{\beta\beta}}{\partial \beta} + H_\alpha H_\beta \frac{\partial \sigma^k_{\beta z}}{\partial z} + \left(\frac{2H_\alpha}{R_\beta} + \frac{H_\beta}{R_\alpha} \right) \sigma^k_{\beta z} = \rho^k H_\alpha H_\beta \ddot{v}^k \ , \tag{2}$$

$$H_\beta \frac{\partial \sigma^k_{\alpha z}}{\partial \alpha} + H_\alpha \frac{\partial \sigma^k_{\beta z}}{\partial \beta} + H_\alpha H_\beta \frac{\partial \sigma^k_{zz}}{\partial z} - \frac{H_\beta}{R_\alpha} \sigma^k_{\alpha\alpha} - \frac{H_\alpha}{R_\beta} \sigma^k_{\beta\beta} + \left(\frac{H_\beta}{R_\alpha} + \frac{H_\alpha}{R_\beta} \right) \sigma^k_{zz} = \rho^k H_\alpha H_\beta \ddot{w}^k \ , \tag{3}$$

where ρ^k indicates the mass density, $(\sigma^k_{\alpha\alpha}, \sigma^k_{\beta\beta}, \sigma^k_{zz}, \sigma^k_{\beta z}, \sigma^k_{\alpha z}, \sigma^k_{\alpha\beta})$ is the stress vector and $\ddot{u}^k$, $\ddot{v}^k$ and $\ddot{w}^k$ mean the second temporal derivatives of the three displacement components u^k, v^k and w^k in α, β and z directions, respectively. Each variable depends on the k layers (the true physical layers embedded in the structure). R_α and R_β are the radii of curvature referred to the mid-surface Ω_0 of the whole multilayered structure. H_α and H_β continuously vary through the thickness of the multilayered shell and they depend on the thickness coordinate z. The middle surface Ω_0 of the shell is the locus of points which lie midway between these surfaces. The parametric coefficients for shells in the case of constant radii of curvature are:

$$H_\alpha = \left(1 + \frac{z}{R_\alpha} \right) \ , \quad H_\beta = \left(1 + \frac{z}{R_\beta} \right) \ , \quad H_z = 1 \ . \tag{4}$$

For simply supported shells and plates, the three displacement components have the following harmonic form:

$$u^j(\alpha, \beta, z, t) = U^j(z) e^{i\omega t} cos(\bar{\alpha}\alpha) sin(\bar{\beta}\beta) \ , \tag{5}$$

$$v^j(\alpha, \beta, z, t) = V^j(z) e^{i\omega t} sin(\bar{\alpha}\alpha) cos(\bar{\beta}\beta) \ , \tag{6}$$

$$w^j(\alpha, \beta, z, t) = W^j(z) e^{i\omega t} sin(\bar{\alpha}\alpha) sin(\bar{\beta}\beta) \ , \tag{7}$$

where $U^j(z)$, $V^j(z)$ and $W^j(z)$ are the displacement amplitudes in α, β and z directions, respectively. The imaginary unit is indicated by i. The circular frequency is $\omega = 2\pi f$ where f is the frequency value measured in Hz and t is the time. The coefficients $\bar{\alpha}$ and $\bar{\beta}$ take the form $\bar{\alpha} = \frac{m\pi}{a}$ and $\bar{\beta} = \frac{n\pi}{b}$, where m and n are the half-wave numbers and a and b are the shell dimensions in α and β directions, respectively (calculated on the mid-surface Ω_0). The index j indicates the mathematical layers used to approximate the curvatures in the k physical layers (each k physical layer is divided in j mathematical layers in order to calculate the parametric coefficients with a sufficient precision). The substitution of Eqs.(5)-(7) and constitutive and geometrical equations (here omitted but given in details in [37] and [39]) in Eqs.(1)-(3) leads to the following final system:

$$\begin{gathered}
\left(-\frac{C^j_{55} H^j_\beta}{H^j_\alpha R^2_\alpha} - \frac{C^j_{55}}{R_\alpha R_\beta} - \bar{\alpha}^2 \frac{C^j_{11} H^j_\beta}{H^j_\alpha} - \bar{\beta}^2 \frac{C^j_{66} H^j_\alpha}{H^j_\beta} + \rho^j H^j_\alpha H^j_\beta \omega^2 \right) U^j + \left(-\bar{\alpha}\bar{\beta} C^j_{12} - \bar{\alpha}\bar{\beta} C^j_{66} \right) V^j + \\
\left(\bar{\alpha} \frac{C^j_{11} H^j_\beta}{H^j_\alpha R_\alpha} + \bar{\alpha} \frac{C^j_{12}}{R_\beta} + \bar{\alpha} \frac{C^j_{55} H^j_\beta}{H^j_\alpha R_\alpha} + \bar{\alpha} \frac{C^j_{55}}{R_\beta} \right) W^j + \left(\frac{C^j_{55} H^j_\beta}{R_\alpha} + \frac{C^j_{55} H^j_\alpha}{R_\beta} \right) U^j_{,z} + \left(\bar{\alpha} C^j_{13} H^j_\beta + \bar{\alpha} C^j_{55} H^j_\beta \right) W^j_{,z} + \\
\left(C^j_{55} H^j_\alpha H^j_\beta \right) U^j_{,zz} = 0 \ ,
\end{gathered} \tag{8}$$

$$\left(-\bar{\alpha}\bar{\beta}C^j_{66}-\bar{\alpha}\bar{\beta}C^j_{12}\right)U^j+\left(-\frac{C^j_{44}H^j_\alpha}{H^j_\beta R^2_\beta}-\frac{C^j_{44}}{R_\alpha R_\beta}-\bar{\alpha}^2\frac{C^j_{66}H^j_\beta}{H^j_\alpha}-\bar{\beta}^2\frac{C^j_{22}H^j_\alpha}{H^j_\beta}+\rho^j H^j_\alpha H^j_\beta\omega^2\right)V^j+$$
$$\left(\bar{\beta}\frac{C^j_{44}H^j_\alpha}{H^j_\beta R_\beta}+\bar{\beta}\frac{C^j_{44}}{R_\alpha}+\bar{\beta}\frac{C^j_{22}H^j_\alpha}{H^j_\beta R_\beta}+\bar{\beta}\frac{C^j_{12}}{R_\alpha}\right)W^j+\left(\frac{C^j_{44}H^j_\alpha}{R_\beta}+\frac{C^j_{44}H^j_\beta}{R_\alpha}\right)V^j_{,z}+\left(\bar{\beta}C^j_{44}H^j_\alpha+\bar{\beta}C^j_{23}H^j_\alpha\right)W^j_{,z}+ \tag{9}$$
$$\left(C^j_{44}H^j_\alpha H^j_\beta\right)V^j_{,zz}=0\,,$$
$$\left(\bar{\alpha}\frac{C^j_{55}H^j_\beta}{H^j_\alpha R_\alpha}-\bar{\alpha}\frac{C^j_{13}}{R_\beta}+\bar{\alpha}\frac{C^j_{11}H^j_\beta}{H^j_\alpha R_\alpha}+\bar{\alpha}\frac{C^j_{12}}{R_\beta}\right)U^j+\left(\bar{\beta}\frac{C^j_{44}H^j_\alpha}{H^j_\beta R_\beta}-\bar{\beta}\frac{C^j_{23}}{R_\alpha}+\bar{\beta}\frac{C^j_{22}H^j_\alpha}{H^j_\beta R_\beta}+\bar{\beta}\frac{C^j_{12}}{R_\alpha}\right)V^j+\left(\frac{C^j_{13}}{R_\alpha R_\beta}+\right.$$
$$\left.\frac{C^j_{23}}{R_\alpha R_\beta}-\frac{C^j_{11}H^j_\beta}{H^j_\alpha R^2_\alpha}-\frac{2C^j_{12}}{R_\alpha R_\beta}-\frac{C^j_{22}H^j_\alpha}{H^j_\beta R^2_\beta}-\bar{\alpha}^2\frac{C^j_{55}H^j_\beta}{H^j_\alpha}-\bar{\beta}^2\frac{C^j_{44}H^j_\alpha}{H^j_\beta}+\rho^j H^j_\alpha H^j_\beta\omega^2\right)W^j+\left(-\bar{\alpha}C^j_{55}H^j_\beta-\right. \tag{10}$$
$$\left.\bar{\alpha}C^j_{13}H^j_\beta\right)U^j_{,z}+\left(-\bar{\beta}C^j_{44}H^j_\alpha-\bar{\beta}C^j_{23}H^j_\alpha\right)V^j_{,z}+\left(\frac{C^j_{33}H^j_\beta}{R_\alpha}+\frac{C^j_{33}H^j_\alpha}{R_\beta}\right)W^j_{,z}+\left(C^j_{33}H^j_\alpha H^j_\beta\right)W^j_{,zz}=0\,.$$

In the case of cylindrical bending analysis, one of the two half-wave numbers (m or n) is set to zero which means $\bar{\alpha}=\frac{m\pi}{a}=0$ or $\bar{\beta}=\frac{n\pi}{b}=0$. This feature gives the derivatives made in a particular direction (α or β) equals zero and each section in the cylindrical bending direction is always the same because quantities do not change in this particular direction. However, this feature is possible only if the side is rectilinear otherwise the curvature presence does not give constant quantities (see Figure 1).

Eqs. (8)-(10) given in compact form are (all the omitted details can be found in [36], [37] and [39]):

$$\boldsymbol{D}^j\frac{\partial\boldsymbol{U}^j}{\partial z}=\boldsymbol{A}^j\boldsymbol{U}^j\,, \tag{11}$$

where $\frac{\partial\boldsymbol{U}^j}{\partial z}=\boldsymbol{U}^{j\prime}$ and $\boldsymbol{U}^j=[U^j\ V^j\ W^j\ U^{j\prime}\ V^{j\prime}\ W^{j\prime}]$. Eq.(11) can be proposed as:

$$\boldsymbol{D}^j\boldsymbol{U}^{j\prime}=\boldsymbol{A}^j\boldsymbol{U}^j\,, \tag{12}$$
$$\boldsymbol{U}^{j\prime}=\boldsymbol{D}^{j-1}\boldsymbol{A}^j\ \boldsymbol{U}^j\,, \tag{13}$$
$$\boldsymbol{U}^{j\prime}=\boldsymbol{A}^{j*}\ \boldsymbol{U}^j\,, \tag{14}$$

with $\boldsymbol{A}^{j*}=\boldsymbol{D}^{j-1}\boldsymbol{A}^j$.

The solution of Eq.(14), as already described in [36], [37] and [39], is:

$$\boldsymbol{U}^j(z^j)=exp(\boldsymbol{A}^{j*}z^j)\boldsymbol{U}^j(0)\quad\text{with}\quad z^j\ \epsilon\ [0,h^j]\,, \tag{15}$$

where z^j is the thickness coordinate for the j layer with values from 0 at the bottom to h^j at the top. The exponential matrix is calculated with $z^j=h^j$ for each j layer as:

$$\boldsymbol{A}^{j**}=exp(\boldsymbol{A}^{j*}h^j)=\boldsymbol{I}+\boldsymbol{A}^{j*}\,h^j+\frac{\boldsymbol{A}^{j*2}}{2!}{h^j}^2+\frac{\boldsymbol{A}^{j*3}}{3!}{h^j}^3+\ldots+\frac{\boldsymbol{A}^{j*N}}{N!}{h^j}^N\,, \tag{16}$$

where $\boldsymbol{I}$ is the 6×6 identity matrix. This expansion has a fast convergence and it is not time consuming from the computational point of view.

Considering $j=M$ mathematical layers to approximate the shell curvature, $M-1$ transfer matrices must be calculated using for each interface the interlaminar continuity conditions of displacements and transverse shear/normal stresses. In order to obtain a closed form solution, the plates or shells must be

considered as simply supported and free stresses at the top and at the bottom surfaces. The following final system is obtained using the described conditions:

$$\boldsymbol{E}\,\boldsymbol{U}^1(0) \;=\; \mathbf{0}\,, \tag{17}$$

dimension of matrix $\boldsymbol{E}$ is (6×6), independently from the number of layers M, even if the solution is based on a layer-wise method. $\boldsymbol{U}^1(0)$ is $\boldsymbol{U}$ considered at the bottom of the entire multilayered structure (first layer 1 with $z^1 = 0$). Further comments about this solution method and all the steps omitted in this work are given in [36]- [44] where this 3D exact solution has been extended for the first time to several cases. The model has been extensively validated in [36]- [44] where it has been compared with several 3D solutions given in the literature for one-layered and multilayered isotropic, orthotropic, composite and FGM plates, cylinders and cylindrical/spherical shells. Therefore, it can be now used with confidence for the frequency comparisons shown in Section 4.

The free vibration analysis is conducted finding the non-trivial solution of $\boldsymbol{U}^1(0)$ in Eq.(17), this feature means the imposition of the determinant of matrix $\boldsymbol{E}$ equals zero:

$$det[\boldsymbol{E}] = 0\,, \tag{18}$$

Eq.(18) allows to calculate the roots of an higher order polynomial in $\lambda = \omega^2$. When a pair of half-wave numbers (m, n) is imposed, a defined number of circular frequency values $\omega = 2\pi f$ (theoretically from I to ∞) is calculated. This number depends on the order N used for the exponential matrix $\boldsymbol{A}^{j**}$ and on the number M of fictitious/mathematical layers used to approximate the shell curvatures. From the validations proposed in [36]- [44] using different cases proposed in the literature, $N = 3$ for the exponential matrix and $M = 100$ or $M = 102$ for the mathematical layers (depending on the number of physical layers embedded in the structure) are sufficient to always calculate the correct results for each geometry, lamination sequence, number of layers, material and thickness ratio.

3 2D numerical models

Two different numerical models are used in the following sections to calculate the 3D exact shell results. The first one is a classic 2D Finite Element (FE) model obtained using a commercial code (Strand7), the second one is an innovative strong form solution achieved using the well-known Generalized Differential Quadrature (GDQ) method [45]. For the sake of conciseness, no details are given regarding the FE solution. The interested readers can refer to the user manual of the cited code for further details. The only important feature is the use of standard 8-node elements, termed QUAD8, for the numerical FE analyses. Data about mesh and convergence analysis can be found in past authors' works [2]- [4]. On the contrary, some details should be given for the GDQ solution because it does not follow the general approach for the study of plates and shells generally used by other researchers. In particular, two main features should be underlined regarding the present GDQ implementation. Firstly, higher order models are used. Secondly, the GDQ shell model includes the curvature effects and the rotary inertias into the formulation. As it is well-known, higher order models reach higher level of accuracy with respect to the 3D analysis if compared to classic linear theories such as Reissner-Mindlin (also known as First order Shear Deformation Theory or FSDT, implemented in most FE codes) and Kirchhoff-Love (theory of moderately thin structures). More accurate results are achieved, when curved structures are analyzed, if the curvature effects are included into the formulation [46].

The present 2D refined kinematic model falls within the general framework of unified formulations [47]- [55] and it can be presented as:

$$\mathbf{U} = \sum_{\tau=0}^{N_e+1} \mathbf{F}_\tau \mathbf{u}^{(\tau)}\,, \tag{19}$$

where $\mathbf{U}$ contains the 3D displacement components and $\mathbf{u}$ includes the displacement parameters of the τth order. It is recalled that these parameters lay on the middle surface of the shell [47]. $\mathbf{F}_{\tau(ij)} = \delta_{ij} F_\tau$ (for $i, j = 1, 2, 3$) is the thickness function matrix and δ is the Kronecker delta function.

Generally power functions are considered through the shell thickness, therefore F_τ takes the form of 1, z, z^2, z^3, according to the order of expansion τ. It is not the aim of the present investigation to show the accuracy among different expansion orders. Thus, for all the following numerical results it has been set $\tau = 0, 1, 2, 3$ and $N_c = 3$, because it has been demonstrated by previous works about similar topics [47]- [55] that this expansion is generally more than enough to obtain accurate solutions for thin and thick shells. When multi-layered structures are considered, the Murakami function is added to the kinematic expansion. It is recalled that the exponent $N_c + 1$ is reserved for the Murakami function, otherwise this order is neglected.

It has been demonstrated in the previous authors' works that the numerical solutions of classic FEs are similar to the ones obtained setting $\tau = 0, 1$ and $N_c = 1$ because a FSDT is achieved, even though the strong form approaches led to more accurate results with respect to the FE ones [51], [53].

The relation between generalized strains $\boldsymbol{\varepsilon}^{(\tau)}$ and displacements $\mathbf{u}^{(\tau)}$ can be set as:

$$\boldsymbol{\varepsilon}^{(\tau)} = \mathbf{D}_\Omega \mathbf{u}^{(\tau)} \quad \text{for} \quad \tau = 0, 1, 2, \ldots, N_c, N_c + 1\,, \tag{20}$$

$\mathbf{D}_\Omega$ is a differential operator explicitly defined in [47]. The present constitutive material model is linear and elastic, therefore for a general kth lamina, the Hooke law can be applied:

$$\boldsymbol{\sigma}^{(k)} = \bar{\mathbf{C}}^{(k)} \boldsymbol{\varepsilon}^{(k)}\,, \tag{21}$$

where $\boldsymbol{\sigma}^{(k)}$ is the vector of the stress components and $\bar{\mathbf{C}}^{(k)}$ is the matrix of elastic coefficients valid for the kth ply [47]. The components of the constitutive matrix are indicated as $\bar{C}^{(k)}_{\xi\eta}$ and are defined with respect to the curvilinear reference system $O'\alpha\beta z$ after the application of the transformation equations [47], that take the elastic constants from the material reference system to the geometrical one.

The Hamilton principle helps to define the stress resultants of the τth order for a 3D doubly-curved solid [47]:

$$\mathbf{S}^{(\tau)} = \sum_{k=1}^{N_L} \int_{z_k}^{z_{k+1}} \left(\mathbf{Z}^{(\tau)}\right)^T \boldsymbol{\sigma}^{(\tau)} H_\alpha H_\beta dz \quad \text{for} \quad \tau = 0, 1, 2, \ldots, N_c, N_c + 1\,, \tag{22}$$

where $\mathbf{S}^{(\tau)}$ is the vector of the τth order which includes the stress resultants. The definition of Eq. (22) can be rewritten as a function of the generalized sth order strain $\boldsymbol{\varepsilon}^{(s)}$ vector as:

$$\mathbf{S}^{(\tau)} = \sum_{s=0}^{N_c+1} \mathbf{A}^{(\tau s)} \boldsymbol{\varepsilon}^{(s)} \quad \text{for} \quad \tau = 0, 1, 2, \ldots, N_c, N_c + 1 \tag{23}$$

where

$$\mathbf{A}^{(\tau s)} = \sum_{k=1}^{N_L} \int_{z_k}^{z_{k+1}} \left(\mathbf{Z}^{(\tau)}\right)^T \bar{\mathbf{C}}^{(k)} \mathbf{Z}^{(s)} H_\alpha H_\beta dz\,. \tag{24}$$

Equation (24) defines the elastic coefficients which are given by the following integral expressions:

$$
\begin{aligned}
A^{(\tau s)}_{\xi\eta(\varrho\zeta)} &= \sum_{k=1}^{N_L}\int_{z_k}^{z_{k+1}} \bar{C}^{(k)}_{\xi\eta} F_s F_\tau \frac{H_\alpha H_\beta}{H^\varrho_\alpha H^\zeta_\beta} dz \\
A^{(\tilde{\tau} s)}_{\xi\eta(\varrho\zeta)} &= \sum_{k=1}^{N_L}\int_{z_k}^{z_{k+1}} \bar{C}^{(k)}_{\xi\eta} F_s \frac{\partial F_\tau}{\partial z} \frac{H_\alpha H_\beta}{H^\varrho_\alpha H^\zeta_\beta} dz \qquad \text{for} \quad \tau, s = 0,1,2,\ldots,N_c,N_c+1 \\
& \qquad\qquad\qquad\qquad\qquad\qquad\qquad\qquad\qquad\qquad\qquad\qquad \text{for} \quad \xi,\eta = 1,2,3,4,5,6 \qquad (25)\\
A^{(\tau \tilde{s})}_{\xi\eta(\varrho\zeta)} &= \sum_{k=1}^{N_L}\int_{z_k}^{z_{k+1}} \bar{C}^{(k)}_{\xi\eta} \frac{\partial F_s}{\partial z} F_\tau \frac{H_\alpha H_\beta}{H^\varrho_\alpha H^\zeta_\beta} dz \qquad \text{for} \quad \varrho,\zeta = 0,1,2 \\
A^{(\tilde{\tau} \tilde{s})}_{\xi\eta(\varrho\zeta)} &= \sum_{k=1}^{N_L}\int_{z_k}^{z_{k+1}} \bar{C}^{(k)}_{\xi\eta} \frac{\partial F_s}{\partial z}\frac{\partial F_\tau}{\partial z} \frac{H_\alpha H_\beta}{H^\varrho_\alpha H^\zeta_\beta} dz
\end{aligned}
$$

where τ, s indicate the corresponding thickness function F_τ, F_s (classic powers of z in this paper). It is recalled that the exponent N_c+1 is reserved for the Murakami function, otherwise this order is neglected. The subscripts $\tilde{\tau}$, $\tilde{s}$ indicate the derivatives of the thickness functions F_τ, F_s with respect to z. Since only power functions have been used, they take the form $\partial F_\tau/\partial z, \partial F_s/\partial z = 0,\ 1,\ 2z,\ 3z^2,\ 4z^3,\ \ldots,\ N_c z^{N_c-1}$. The subscripts ϱ, ζ represent the exponent of the quantities H_α, H_β, whereas ξ, η are the indices of the material constants $\bar{C}^{(k)}_{\xi\eta}$ for the kth ply [47]- [54].

The dynamic equilibrium equations and their boundary conditions are carried out from the Hamilton Principle. The present generalized approach gives a fundamental nucleus of three motion equations:

$$
\mathbf{D}^\star_\Omega \mathbf{S}^{(\tau)} = \sum_{s=0}^{N_c+1} \mathbf{M}^{(\tau s)} \ddot{\mathbf{u}}^{(s)} \quad \text{for} \quad \tau = 0,1,2,\ldots,N_c,N_c+1\,, \tag{26}
$$

where $\mathbf{D}^\star_\Omega$ is the equilibrium operator and $\mathbf{M}^{(\tau s)}$ is the inertia matrix. Their explicit expressions have been presented in a previous authors' paper [47].

By combining the kinematic equation (20), constitutive equation (23) and the motion equation (26), the fundamental governing system in terms of displacement parameters is carried out:

$$
\sum_{s=0}^{N_c+1} \mathbf{L}^{(\tau s)} \mathbf{u}^{(s)} = \sum_{s=0}^{N_c+1} \mathbf{M}^{(\tau s)} \ddot{\mathbf{u}}^{(s)} \quad \text{for} \quad \tau = 0,1,2,\ldots,N_c,N_c+1\,, \tag{27}
$$

where $\mathbf{L}^{(\tau s)} = \mathbf{D}^\star_\Omega \mathbf{A}^{(\tau s)} \mathbf{D}_\Omega$ is the fundamental operator [47].

Boundary conditions must be included for the solution of the differential equations (27). Combining conveniently the static and kinematic conditions, any boundary condition can be imposed. In general, three possibilities are the most used ones [47], which are: clamped edge boundary conditions (C), free edge boundary conditions (F) and simply-supported edge boundary conditions (S). The present paper investigates structures with simply-supported and free edges. Thus, simply supported conditions are:

$$
\begin{aligned}
&N^{(\tau)}_\alpha = 0,\ u^{(\tau)}_\beta = u^{(\tau)}_z = 0 \quad \tau = 0,1,2,\ldots,N_c,N_c+1 \quad \text{at} \quad \alpha = \alpha^0 \quad \text{or} \quad \alpha = \alpha^1 \quad \beta^0 \le \beta \le \beta^1\,, \\
&u^{(\tau)}_\alpha = 0,\ N^{(\tau)}_\beta = 0,\ u^{(\tau)}_z = 0 \quad \tau = 0,1,2,\ldots,N_c,N_c+1 \quad \text{at} \quad \beta = \beta^0 \quad \text{or} \quad \beta = \beta^1 \quad \alpha^0 \le \alpha \le \alpha^1\,,
\end{aligned} \tag{28}
$$

whereas the free edge conditions can be indicated as:

$$
\begin{aligned}
&N^{(\tau)}_\alpha = 0,\ N^{(\tau)}_\beta = 0,\ T^{(\tau)}_\alpha = 0 \quad \tau = 0,1,2,\ldots,N_c,N_c+1 \quad \text{at} \quad \alpha = \alpha^0 \quad \text{or} \quad \alpha = \alpha^1 \quad \beta^0 \le \beta \le \beta^1\,, \\
&N^{(\tau)}_\alpha = 0,\ N^{(\tau)}_\beta = 0,\ T^{(\tau)}_\beta = 0 \quad \tau = 0,1,2,\ldots,N_c,N_c+1 \quad \text{at} \quad \beta = \beta^0 \quad \text{or} \quad \beta = \beta^1 \quad \alpha^0 \le \alpha \le \alpha^1\,.
\end{aligned} \tag{29}
$$

Each of the investigated structures in Section 4 has four edges. In the original case, the four edges are simply-supported as reported by Eqs.(28). In order to perform the cylindrical bending analyses, two edges are simply-supported and the other two are free. Therefore, Eqs. (28) and (29) are mixed accordingly to the problem under investigation. Refer to each single problem of the Section 4 for more details on these features.

4 Results

In this section, the numerical results regarding the comparison of Cylindrical Bending (C.B.) effects of 3D exact shell models and 2D numerical ones are presented. This paper focuses on flat plates, circular cylinders and cylindrical shells because the C.B. effects occur only when at least two straight edges are present (see Figure 1 for further details).

The first example regards a simply-supported square plate ($a = b = 1$ m) with thickness ratios a/h equal 100 and 20. Thin and moderately thick plates are drawn. The structure is one-layered ($h_1 = h$) and made of Aluminum alloy ($E = 73$ GPa, $\nu = 0.3$, $\rho = 2800$ kg/m^3). The FE model uses a 40×40 QUAD8 mesh with a total number of 29280 degrees of freedom (dofs). The GDQ solution is based on a not-uniform grid (Chebyshev-Gauss-Lobatto collocation [45]) with 31×31 points for both thin and moderately thick plates and a third-order kinematic model without Murakami function. All the results are reported in Table 1 where the first column indicates the half-wave numbers to set in the 3D exact shell model. The second column indicates the type of mode for the 3D exact solution for a given (m, n) couple. I indicates the first mode and II indicates the second mode. In the case of in-plane modes, the caption ($w = 0$) is added. The third column shows all the results for the 3D exact solution, both classical and cylindrical bending (C.B.) results are obtained using the same run. The other four columns of the table are related to the 2D numerical models where simply-supported four edges conditions are investigated through 2D FE and 2D GDQ models, and cylindrical bending results are calculated via 2D FE(C.B.) and 2D GDQ(C.B.) models. The numerical results related to the full simply-supported boundary conditions are found implementing a single numerical model where the four edges are simply supported. The same conditions cannot be used for the C.B. results due to symmetry. In order to achieve two different mode shapes in cylindrical bending, two different structures must be numerically modeled. For instance, in order to get the mode shapes related to $(0, 1)$ or $(1, 0)$, the β edges must be free or the α edges must be free, respectively. The same can be said for all the other symmetric conditions in cylindrical bending. It must be underlined that there is a perfect match among the 3D and 2D solutions when full simply-supported structures are analyzed. On the contrary, a small error is observed for the C.B. conditions. This aspect is due to the fact that the numerical models do not achieve a perfect cylindrical bending mode shape, as the 3D exact model, and this feature is clearly shown in Figures 2 and 3. This behavior happens because the C.B. deformed shape must have the derivatives along the simply supported direction equals zero and this is not the case of the investigated square plate. In fact, the color map of the cited figures clearly shows that near the boundaries the flexural displacements are not parallel. The same cannot be said for the in-plane mode shapes ($w = 0$) when the plate is simply-supported on the four edges. In fact, in the latter configuration, the color map depicts parallel color lines and the vibration numerical frequencies perfectly match the 3D exact ones. The perfect C.B. effect occurs when the straight direction has an "infinite" length. Obviously this aspect cannot be numerically proven, but a trend to such solution can be found extending the length of the simply-supported edges, as it is reported in Table 2 and in Figures 4 and 5. Table 2 reports the values of the first natural frequency of the $a/h = 100$ plate that has two simply-supported edges and two free edges using the GDQ model. a is the plate side and L is the extended edge. Table 2 is reported in graphical form in Figure 4 where it is clear that the more L is large, the smaller is the error with respect to the 3D exact model. When the considered edge is 25 times the original one, the error between the two solutions is very small. In fact, the mode shape for such structure is very similar to

a C.B. condition as depicted by Figure 5, in this case the boundary effects are negligible with respect the length of the simply supported edges. Take note that it is not possible to completely avoid the boundary effects due to the free edges. Results with $m = 0$ or $n = 0$ combined with $w = 0$ are not cylindrical bending modes and they can be found with 2D numerical models without modifying the boundary conditions.

The second case considers the same plate geometry described in the first example. In this case four composite layers with the same thickness ($h_1 = h_2 = h_3 = h_4 = h/4$) and lamination sequence $90°/0°/90°/0°$ are considered. The material properties are $E_1 = 132.38$ GPa, $E_2 = E_3 = 10.756$ GPa, $\nu_{12} = \nu_{13} = 0.24$ and $\nu_{23} = 0.49$, shear modulus $G_{12} = G_{13} = 5.6537$ GPa and $G_{23} = 3.603$ GPa, $\rho = 1600$ kg/m^3. Both numerical 2D models (FE and GDQ ones) use the same elements, mesh, grid and degrees of freedom already shown in the first example. The Murakami zigzag function is added to the refined 2D GDQ model in the case of multilayered configurations. Results are proposed in Table 3 using the same organization already described for the Table 1. The conclusions and considerations already seen for the one-layered isotropic plate analyzed in Table 1 are confirmed for the four-layered composite plate investigated in Table 3. For the composite lamination, the refined 2D GDQ model is much closer to 3D exact solution than the classical 2D FE model.

The third example is related to a simply-supported cylinder with $R_\alpha = 10$ m, $R_\beta = \infty$, $a = 2\pi R_\alpha$, $b = 20$ m and thickness ratios R_α/h equals 100 and 10. A two-layer lamination scheme is taken into account with $h_1 = h_2 = h/2$ made of Aluminium alloy as bottom layer and Titanium alloy ($E = 114$ GPa, $\nu = 0.3$, $\rho = 2768$ kg/m^3) as top layer. The FE model is made of 20×80 QUAD8 elements for a total number of 27966 degrees of freedom, whereas the GDQ solution is made of a 21×41 Chebyshev-Gauss-Lobatto grid. The results for this example are reported in Table 4 with the same meaning of the columns already seen in the previous flat plate cases. It should be noted that the structure is symmetric only with respect to one direction. Numerically speaking, compatibility conditions must be enforced on the closing meridian in order to obtain a closed revolution shell. Thus, for achieving C.B. conditions the shell is numerically investigated as not bounded. In this case the first 6 mode shapes (rigid body motions) are neglected and the other flexural modes are taken from the 7th numerical mode onwards. Good agreement can be observed among all the presented vibration frequencies. Results with $n = 0$ and $w \neq 0$ indicate the C.B. conditions. Such results are obtained by means of 2D numerical models modifying the boundary conditions (see 2D FE(C.B.) and 2D GDQ(C.B.) models). The cases $n = 0$ combined with $w = 0$ are not C.B. conditions and the frequencies can be found without modifying the boundary conditions in the 2D numerical models.

The final test regards a simply-supported cylindrical shell panel with $R_\alpha = 10$ m, $R_\beta = \infty$, $a = \pi/3R_\alpha$, $b = 20$ m and thickness ratios R_α/h equals 100 and 10. The structure is made of a three-layered ($h_1 = h_2 = h_3 = h/3$) composite laminate with $90°/0°/90°$ sequence and material properties $E_1 = 132.38$ GPa, $E_2 = E_3 = 10.756$ GPa, $\nu_{12} = \nu_{13} = 0.24$ and $\nu_{23} = 0.49$, shear modulus $G_{12} = G_{13} = 5.6537$ GPa and $G_{23} = 3.603$ GPa, $\rho = 1600$ kg/m^3 (the same material proposed for the composite plate case). The FE model is made of 40×40 QUAD8 elements for total 29280 degrees of freedom, whereas the GDQ solution is made of a 31×31 Chebyshev-Gauss-Lobatto grid. The present natural frequencies are reported in Table 5 with the same meaning of the columns seen in the previous cases. In order to achieve the cylindrical bending conditions, the numerical models have the straight edges simply-supported and the curved ones as free. Note that it is not possible to achieve C.B. conditions when (m, n) equals $(0, 1)$ or $(0, 2)$ because the cylindrical bending should occur on the curved edge and this is not physically possible because of the variation of displacement components due to the curvature presence. This feature is indicated as N.A. (Not Applicable) solution in Table 5. Therefore, this kind of 3D exact solutions cannot be achieved by any numerical model. Cases with $n = 0$ or $m = 0$ combined with $w = 0$ can be found with 2D numerical models without modifying the simply supported boundary conditions.

5 Conclusions

This work presented the cylindrical bending of plates and cylindrical shells in the free vibration analysis. This effect is analyzed using a 3D exact shell model and two different 2D numerical models, one based on the weak formulation (classical FEs) and the other one based on the strong formulation (GDQ method). It has been demonstrated that the cylindrical bending (C.B.) behavior in the 3D exact shell model can be achieved considering completely simply-supported structures and simply imposing one of the two half-wave numbers equals zero. The numerical models need mixed simply-supported and free boundary conditions in order to obtain the cylindrical bending behavior. It has been shown that the actual cylindrical bending (C.B.) occurs only with respect to straight edges. The C.B. natural frequencies of the numerical solutions tend to the 3D exact ones when the straight simply-supported edges are extended up to 20 times the value of the original edges. The C.B. conditions cannot be obtained modifying the boundary conditions in 2D numerical models when the half-wave number is zero in the curvilinear edge. In-plane vibration modes with $m = 0$ or $n = 0$ combined with zero transverse displacement are not C.B. modes and they can be obtained by 2D numerical models without modifying the simply supported conditions for all the edges.

References

[1] S. Brischetto and R. Torre, Exact 3D solutions and finite element 2D models for free vibration analysis of plates and cylinders, *Curved and Layered Structures*, 1, 59-92, 2014.

[2] F. Tornabene, S. Brischetto, N. Fantuzzi and E. Viola, Numerical and exact models for free vibration analysis of cylindrical and spherical shell panels, *Composites part B: engineering*, 81, 231-250, 2015.

[3] S. Brischetto, F. Tornabene, N. Fantuzzi and E. Viola, 3D exact and 2D generalized differential quadrature models for free vibration analysis of functionally graded plates and cylinders, *Meccanica*, 51, 2059-2098, 2016.

[4] N. Fantuzzi, S. Brischetto, F. Tornabene and E. Viola, 2D and 3D shell models for the free vibration investigation of functionally graded cylindrical and spherical panels, *Composite Stuctures*, 154, 573-590, 2016.

[5] W.Q. Chen, J.B. Cai and G.R. Ye, Responses of cross-ply laminates with viscous interfaces in cylindrical bending, *Computer Methods in Applied Mechanics and Engineering*, 194, 823-835, 2005.

[6] W.Q. Chen and K.Y. Lee, Three-dimensional exact analysis of angle-ply laminates in cylindrical bending with interfacial damage via state-space method, *Composite Structures*, 64, 275-283, 2004.

[7] W.Q. Chen and K.Y. Lee, Time-dependent behaviors of angle-ply laminates with viscous interfaces in cylindrical bending, *European Journal of Mechanics A/Solids*, 23, 235-245, 2004.

[8] A.H. Gandhi and H.K. Raval, Analytical and empirical modeling of top roller position for three-roller cylindrical bending of plates and its experimental verification, *Journal of Materials Processing Technology*, 197, 268-278, 2008.

[9] S. Oral and H. Darendeliler, The optimum die profile for the cylindrical bending of plates, *Journal of Materials Processing Technology* 70, 151-155, 1997.

[10] V.A. Jairazbhoy, P. Petukhov and J. Qu, Large deflection of thin plates in cylindrical bending - Non-unique solutions, *International Journal of Solids and Structures*, 45, 3203-3218, 2008.

[11] A. Lebe and K. Sab, A bending-gradient model for thick plates, Part II: closed-form solutions for cylindrical bending of laminates, *International Journal of Solids and Structures*, 48, 2889-2901, 2011.

[12] P.V. Nimbolkar and I.M. Jain, Cylindrical bending of elastic plates, *Procedia Materials Science* 10, 793-802, 2015.

[13] A.S. Sayyad and Y.M. Ghugal, A nth-order shear deformation theory for composite laminates in cylindrical bending, *Curved and Layered Structures* 2, 290-300, 2015.

[14] N.J. Pagano, Exact solutions for composite laminates in cylindrical bending, *Journal of Composite Materials* 3, 398-411, 1969.

[15] N.J. Pagano and A.S.D. Wang, Further study of composite laminates under cylindrical bending, *Journal of Composite Materials* 5, 521-528, 1971.

[16] N. Saeedi, K. Sab and J.-F. Caron, Cylindrical bending of multilayered plates with multi-delamination via a layerwise stress approach, *Composite Structures* 95, 728-739, 2013.

[17] X.-P. Shua and K.P. Soldatos, Cylindrical bending of angle-ply laminates subjected to different sets of edge boundary conditions, *International Journal of Solids and Structures* 37, 4289-4307, 2000.

[18] Z.G. Bian, W.Q. Chen, C.W. Lim and N. Zhang, Analytical solutions for single- and multi-span functionally graded plates in cylindrical bending, *International Journal of Solids and Structures*, 42, 6433-6456, 2005.

[19] H.M. Navazi and H. Haddadpour, Nonlinear cylindrical bending analysis of shear deformable functionally graded plates under different loadings using analytical methods, *International Journal of Mechanical Sciences* 50, 1650-1657, 2008.

[20] W.Q. Chen, J. Ying, J.B. Cai and G.R. Ye, Benchmark solution of imperfect angle-ply laminated rectangular plates in cylindrical bending with surface piezoelectric layers as actuator and sensor, *Computers and Structures*, 82, 1773-1784, 2004.

[21] W.Q. Chen and K.Y. Lee, Exact solution of angle-ply piezoelectric laminates in cylindrical bending with interfacial imperfections, *Composite Structures*, 65, 329-337, 2004.

[22] T. Kant and S.M. Shiyekar, Cylindrical bending of piezoelectric laminates with a higher order shear and normal deformation theory, *Computers and Structures*, 86, 1594-1603, 2008.

[23] P. Lu, H.P. Lee and C. Lu, An exact solution for functionally graded piezoelectric laminates in cylindrical bending, *International Journal of Mechanical Sciences*, 47, 437-458, 2005.

[24] W. Yan, J. Wang and W.Q. Chen, Cylindrical bending responses of angle-ply piezoelectric laminates with viscoelastic interfaces, *Applied Mathematical Modelling* 38, 6018-6030, 2014.

[25] Y.Y. Zhou, W.Q. Chen and C.F. Lu, Semi-analytical solution for orthotropic piezoelectric laminates in cylindrical bending with interfacial imperfections, *Composite Structures* 92, 1009-1018, 2010.

[26] G.P. Dube, S. Kapuria and P.C. Dumir, Exact piezothermoelastic solution of a simply-supported orthotropic flat panel in cylindrical bending, *International Journal of Mechanical Sciences*, 38, 374-387, 1996.

[27] V.N. Pilipchuk, V.L. Berdichevsky and R.A. Ibrahim, Thermo-mechanical coupling in cylindrical bending of sandwich plates, *Composite Structures* 92, 2632-2640, 2010.

[28] C. Zhang, S. Di and N. Zhang, A new procedure for static analysis of thermo-electric laminated composite plates under cylindrical bending, *Composite Structures* 56, 131-140, 2002.

[29] W.Q. Chen and K.Y. Lee, State-space approach for statics and dynamics of angle-ply laminated cylindrical panels in cylindrical bending, *International Journal of Mechanical Sciences*, 47, 374-387, 2005.

[30] C.-P. Wu and Y.-S. Syu, Exact solutions of functionally graded piezoelectric shells under cylindrical bending, *International Journal of Solids and Structures* 44, 6450-6472, 2007.

[31] W. Yan, J. Ying and W.Q. Chen, The behavior of angle-ply laminated cylindrical shells with viscoelastic interfaces in cylindrical bending, *Composite Structures* 78, 551-559, 2007.

[32] G.G. Sheng and X. Wang, Thermoelastic vibration and buckling analysis of functionally graded piezoelectric cylindrical shells, *Applied Mathematical Modelling* 34, 2630-2643, 2010.

[33] G.G. Sheng and X. Wang, Active control of functionally graded laminated cylindrical shells, *Composite Structures* 90, 448457, 2009.

[34] G.G. Sheng and X. Wang, Studies on dynamic behavior of functionally graded cylindrical shells with PZT layers under moving loads, *Journal of Sound and Vibration* 323, 772-789, 2009.

[35] G.G. Sheng and X. Wang, Dynamic characteristics of fluid-conveying functionally graded cylindrical shells under mechanical and thermal loads, *Composite Structures* 93, 162170, 2010.

[36] S. Brischetto, Exact elasticity solution for natural frequencies of functionally graded simply-supported structures, *Computer Modeling in Engineering & Sciences* 95, 391-430, 2013.

[37] S. Brischetto, Three-dimensional exact free vibration analysis of spherical, cylindrical, and flat one-layered panels, *Shock and Vibration* vol. 2014, 1-29, 2014.

[38] S. Brischetto, A continuum elastic three-dimensional model for natural frequencies of single-walled carbon nanotubes, *Composites part B: engineering* 61, 222-228, 2014.

[39] S. Brischetto, An exact 3D solution for free vibrations of multilayered cross-ply composite and sandwich plates and shells, *International Journal of Applied Mechanics* 66, 1-42, 2014.

[40] S. Brischetto, A continuum shell model including van derWaals interaction for free vibrations of double-walled carbon nanotubes, *Computer Modeling in Engineering & Sciences* 104, 305-327, 2015.

[41] S. Brischetto, F. Tornabene, N. Fantuzzi and M. Bacciocchi, Refined 2D and exact 3D shell models for the free vibration analysis of single- and double-walled carbon nanotubes, *Technologies* 3, 259-284, 2015.

[42] S. Brischetto, Convergence analysis of the exponential matrix method for the solution of 3D equilibrium equations for free vibration analysis of plates and shells, *Composites part B: engineering* 98, 453-471, 2016.

[43] S. Brischetto, Exact and approximate shell geometry in the free vibration analysis of one-layered and multilayered structures, *International Journal of Mechanical Sciences* 113, 81-93, 2016.

[44] S. Brischetto, Curvature approximation effects in the free vibration analysis of functionally graded shells, *International Journal of Applied Mechanics*, in press.

[45] F. Tornabene, N. Fantuzzi, F. Ubertini and E. Viola, Strong formulation finite element method based on differential quadrature: a survey, *Applied Mechanics Reviews* 67, 020801-1-55, 2015.

[46] E. Viola, F. Tornabene, Free vibrations of three parameter functionally graded parabolic panels of revolution, *Mechanics Research Communications* 36, 587-594, 2009.

[47] F. Tornabene, E. Viola and N. Fantuzzi, General higher-order equivalent single layer theory for free vibrations of doubly-curved laminated composite shells and panels, *Composite Structures*, 104, 94-117, 2013.

[48] F. Tornabene, N. Fantuzzi, E. Viola and A.J.M. Ferreira, Radial basis function method applied to doubly-curved laminated composite shells and panels with a general higher-order equivalent single layer theory, *Composites part B: engineering*, 55, 642-659, 2013.

[49] F. Tornabene, N. Fantuzzi and M. Bacciocchi, Free vibrations of free-form doubly-curved shells made of functionally graded materials using higher-order equivalent single layer theories, *Composites part B: engineering*, 67, 490-509, 2014.

[50] F. Tornabene, N. Fantuzzi and M. Bacciocchi, The local GDQ method applied to general higher-order theories of doubly-curved laminated composite shells and panels: the free vibration analysis, *Composite Structures*, 116, 637-660, 2014.

[51] F. Tornabene, N. Fantuzzi, M. Bacciocchi and R. Dimitri, Dynamic analysis of thick and thin elliptic shell structures made of laminated composite materials, *Composite Structures*, 133, 278-299, 2015.

[52] F. Tornabene, N. Fantuzzi, M. Bacciocchi and E. Viola, Higher-order theories for the free vibration of doubly-curved laminated panels with curvilinear reinforcing fibers by means of a local version of the GDQ method, *Composites part B: engineering* 81, 196-230, 2015.

[53] F. Tornabene, N. Fantuzzi, M. Bacciocchi and R. Dimitri Free vibrations of composite oval and elliptic cylinders by the generalized differential quadrature method, *Thin-Walled Structures* 97, 114-129, 2015.

[54] F. Tornabene, N. Fantuzzi and M. Bacciocchi, The local GDQ method for the natural frequencies of doubly-curved shells with variable thickness: a general formulation, *Composites part B: engineering* 92, 265-289, 2016.

[55] F. Tornabene, N. Fantuzzi, M. Bacciocchi, A.M.A. Neves and A.J.M. Ferreira, MLSDQ based on RBFs for the free vibrations of laminated composite doubly-curved shells, *Composites part B: engineering* 99, 30-47, 2016.

a/h=100						
m,n	Mode	3D Exact	2D FE	2D FE(C.B.)	2D GDQ	2D GDQ(C.B.)
0,1	I	24.27	-	23.68	-	23.67
1,0	I	24.27	-	23.68	-	23.67
1,1	I	48.52	48.53	-	48.53	-
0,2	I	97.02	-	95.68	-	95.67
2,0	I	97.02	-	95.68	-	95.67
1,2	I	121.2	121.3	-	121.2	-
2,1	I	121.2	121.3	-	121.2	-
2,2	I	193.9	194.0	-	193.9	-
0,3	I	218.1	-	216.0	-	216.0
3,0	I	218.1	-	216.0	-	216.0
1,3	I	242.3	242.7	-	242.3	-
3,1	I	242.3	242.7	-	242.3	-
2,3	I	314.8	315.1	-	314.8	-
3,2	I	314.8	315.1	-	314.8	-
0,4	I	387.3	-	384.2	-	384.3
4,0	I	387.3	-	384.2	-	384.3
1,4	I	411.4	412.6	-	411.4	-
4,1	I	411.4	412.6	-	411.4	-
a/h=20						
m,n	Mode	3D Exact	2D FE	2D FE(C.B.)	2D GDQ	2D GDQ(C.B.)
0,1	I	120.8	-	117.7	-	117.8
1,0	I	120.8	-	117.7	-	117.8
1,1	I	240.6	241.0	-	240.6	-
0,2	I	477.2	-	469.7	-	470.0
2,0	I	477.2	-	469.7	-	470.0
1,2	I	594.0	596.6	-	594.0	-
2,1	I	594.0	596.6	-	594.0	-
2,2	I	938.9	944.7	-	939.0	-
0,3	I	1052	-	1039	-	1041
3,0	I	1052	-	1039	-	1041
1,3	I	1164	1174	-	1164	-
3,1	I	1164	1174	-	1164	-
2,3	I	1496	1511	-	1496	-
3,2	I	1496	1511	-	1496	-
0,1	II (w=0)	1583	1584	-	1583	-
1,0	II (w=0)	1583	1584	-	1583	-
0,4	I	1821	-	1789	-	1805
4,0	I	1821	-	1789	-	1805

Table 1: Isotropic one-layered plate. Analytical 3D vs. 2D numerical models. Frequency f in Hz.

L/a	1	2	3	4	5	6	7	8	9	10	20	25
3D exact	24.27	24.27	24.27	24.27	24.27	24.27	24.27	24.27	24.27	24.27	24.27	24.27
2D GDQ(C.B.)	23.67	23.93	24.03	24.08	24.11	24.13	24.15	24.16	24.17	24.17	24.20	24.20

Table 2: First mode for a/h=100 isotropic plate: convergence of the 2D GDQ(C.B.) solution versus the length of the simply supported edges.

a/h=100						
m,n	Mode	3D Exact	2D FE	2D FE(C.B.)	2D GDQ	2D GDQ(C.B.)
0,1	I	28.24	-	28.23	-	28.23
1,0	I	28.24	-	28.23	-	28.23
1,1	I	44.06	44.08	-	44.07	-
0,2	I	112.7	-	112.7	-	112.6
2,0	I	112.7	-	112.7	-	112.6
1,2	I	121.9	122.1	-	122.0	-
2,1	I	121.9	122.1	-	122.0	-
2,2	I	175.7	175.9	-	175.7	-
0,3	I	252.4	-	252.9	-	252.4
3,0	I	252.4	-	252.9	-	252.4
1,3	I	259.9	260.6	-	260.0	-
3,1	I	259.9	260.6	-	260.0	-
2,3	I	297.7	298.3	-	297.8	-
3,2	I	297.7	298.3	-	297.8	-
3,3	I	393.3	394.3	-	393.4	-
0,4	I	446.0	-	447.8	-	446.1
4,0	I	446.0	-	447.8	-	446.1
1,4	I	452.9	454.7	-	453.1	-
a/h=20						
m,n	Mode	3D Exact	2D FE	2D FE(C.B.)	2D GDQ	2D GDQ(C.B.)
0,1	I	138.3	-	139.2	-	138.3
1,0	I	138.3	-	139.2	-	138.3
1,1	I	215.0	216.5	-	215.1	-
0,2	I	521.6	-	534.0	-	522.6
2,0	I	521.6	-	534.0	-	522.6
1,2	I	565.1	577.8	-	566.3	-
2,1	I	565.1	577.8	-	566.3	-
2,2	I	802.5	821.9	-	804.0	-
0,1	II(w=0)	939.9	939.9	-	939.9	-
1,0	II(w=0)	939.9	939.9	-	939.9	-
0,3	I	1079	-	1128	-	1084
3,0	I	1079	-	1128	-	1084
1,3	I	1112	1162	-	1117	-
3,1	I	1112	1162	-	1117	-
2,3	I	1276	1327	-	1280	-
3,2	I	1276	1327	-	1280	-
3,3	I	1642	1714	-	1647	-
0,4	I	1743	-	1857	-	1753

Table 3: Four-layered composite [90°/0°/90°/0°] plate. Analytical 3D vs. 2D numerical models. Frequency f in Hz.

R_α/h=100						
m,n	Mode	3D Exact	2D FE	2D FE(C.B.)	2D GDQ	2D GDQ(C.B.)
6,0	I	2.078	-	2.072	-	2.070
8,0	I	3.984	-	3.973	-	3.969
10,0	I	6.442	-	6.424	-	6.429
12,0	I	9.448	-	9.423	-	9.428
10,1	I	10.76	10.76	-	10.76	-
12,1	I	11.65	11.64	-	11.65	-
8,1	I	12.77	12.78	-	12.78	-
14,0	I	13.00	-	12.97	-	12.95
14,1	I	14.33	14.31	-	14.33	-
16,0	I	17.10	-	17.06	-	17.03
16,1	I	18.07	18.05	-	18.07	-
6,1	I	18.92	18.93	-	18.93	-
18,0	I	21.74	-	21.70	-	21.65
14,2	I	21.86	21.81	-	21.87	-
R_α/h=10						
m,n	Mode	3D Exact	2D FE	2D FE(C.B.)	2D GDQ	2D GDQ(C.B.)
4,0	I	7.276	-	7.205	-	7.237
6,0	I	20.39	-	20.32	-	20.20
6,1	I	32.11	32.07	-	32.11	-
4,1	I	34.21	34.21	-	34.21	-
8,0	I	38.62	-	38.85	-	38.31
8,1	I	45.94	45.89	-	45.95	-
2,1	I	55.77	55.81	-	55.77	-
2,0	I (w=0)	57.07	57.05	-	57.07	-
10,0	I	61.55	-	62.10	-	61.17
6,2	I	64.74	65.01	-	64.74	-
10,1	I	67.78	67.80	-	67.78	-
4,2	I	70.94	71.37	-	70.94	-
8,2	I	71.41	71.52	-	71.41	-
2,2	I	85.43	86.03	-	85.43	-

Table 4: Isotropic two-layered cylinder. Analytical 3D vs. 2D numerical models. Frequency f in Hz.

R_α/h=100						
m,n	Mode	3D Exact	2D FE	2D FE(C.B.)	2D GDQ	2D GDQ(C.B.)
1,0	I	1.079	-	1.079	-	1.079
2,0	I	4.906	-	4.909	-	4.907
2,1	I	7.717	7.723	-	7.718	-
3,0	I	11.29	-	11.30	-	11.29
3,1	I	12.02	12.02	-	12.02	-
1,1	I	13.43	13.44	-	13.43	-
3,2	I	15.60	15.60	-	15.60	-
2,2	I	15.61	15.62	-	15.62	-
4,0	I	20.21	-	20.25	-	20.21
4,1	I	20.62	20.63	-	20.62	-
3,3	I	21.62	21.62	-	21.62	-
4,2	I	22.52	22.53	-	22.52	-
2,3	I	24.42	24.42	-	24.43	-
4,3	I	26.49	26.49	-	26.49	-
R_α/h=10						
m, n	Mode	3D Exact	2D FE	2D FE(C.B.)	2D GDQ	2D GDQ(C.B.)
1,0	I	10.61	-	10.76	-	10.61
1,1	I	20.81	20.73	-	20.82	-
2,0	I	45.79	-	48.43	-	45.85
0,1	I(w=0)	46.99	47.03	-	46.99	-
1,2	I	47.28	47.11	-	47.30	-
2,1	I	49.51	49.23	-	49.60	-
2,2	I	65.53	65.08	-	65.60	-
1,3	I	82.06	81.73	-	82.09	-
1,0	II(w=0)	89.79	89.80	-	89.79	-
0,1	II	90.69	-	N.A.	-	N.A.
0,2	I(w=0)	93.99	93.99	-	93.99	-
2,3	I	93.94	95.14	-	94.00	-
0,2	II	96.87	-	N.A.	-	N.A.
3,0	I	97.86	-	109.6	-	98.19

Table 5: Three-layered composite [90°/0°/90°] cylindrical shell panel. Analytical 3D vs. 2D numerical models. Frequency f in Hz.

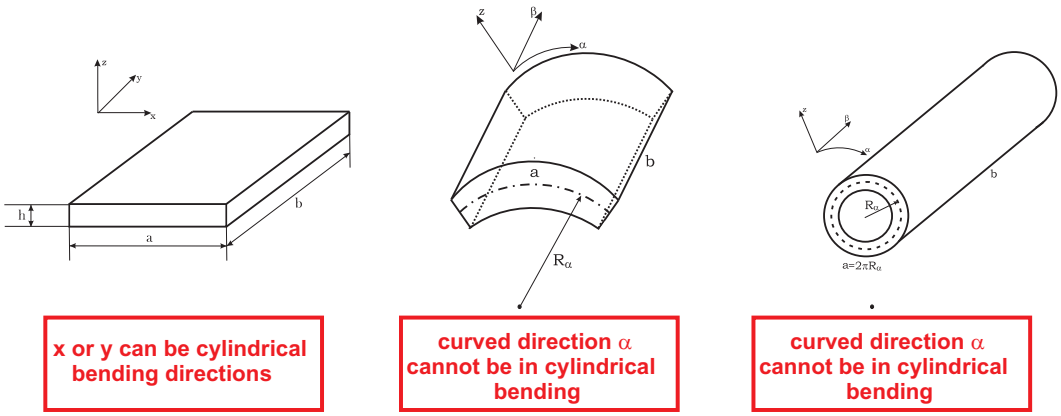

Figure 1: Geometries investigated by means of 3D exact and 2D numerical models.

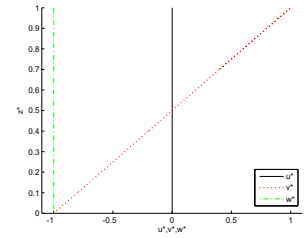

(a) Mode I - (0,1) - 3D

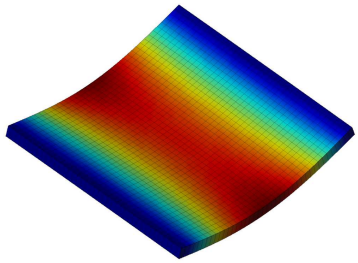

(b) Mode I - (0,1) - 2D

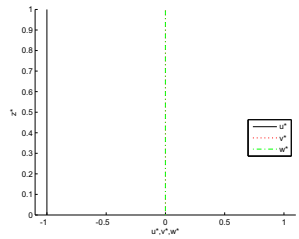

(c) Mode II (w=0) - (0,1) - 3D

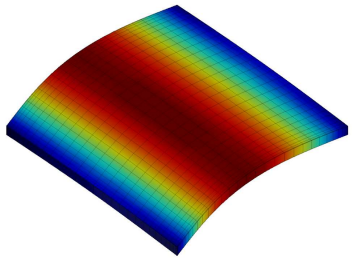

(d) Mode II (w=0) - (0,1) - 2D

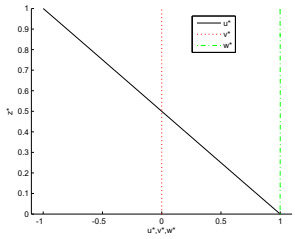

(e) Mode I - (1,0) - 3D

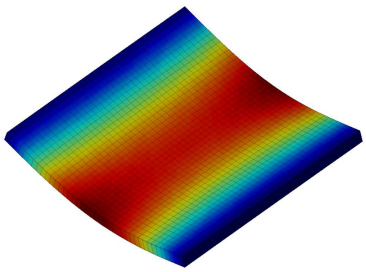

(f) Mode I - (1,0) - 2D

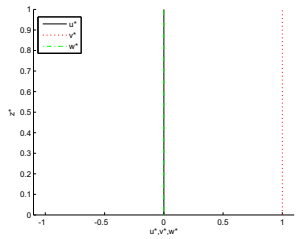

(g) Mode II (w=0) - (1,0) - 3D

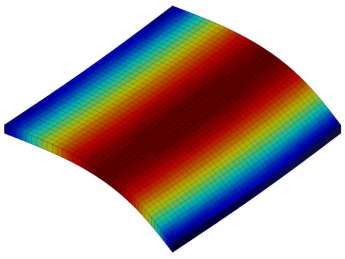

(h) Mode II (w=0) - (1,0) - 2D

Figure 2: Differences between in-plane ($w = 0$) and cylindrical bending vibration modes for the a/h=20 isotropic one-layered plate. 3D modes vs. 2D modes.

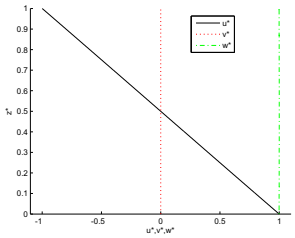

(a) Mode I - (1,0) - 3D

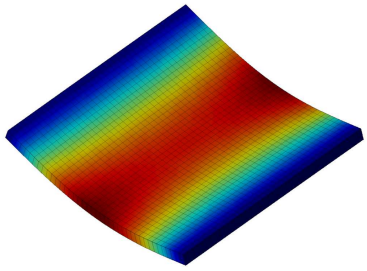

(b) Mode I - (1,0) - 2D

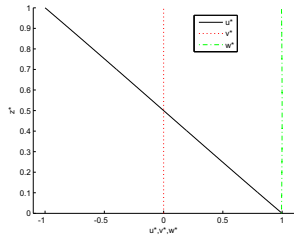

(c) Mode I - (2,0) - 3D

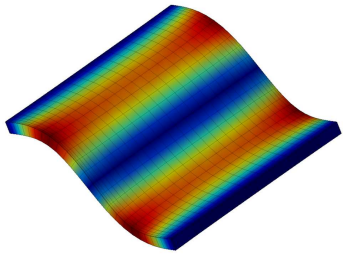

(d) Mode I - (2,0) - 2D

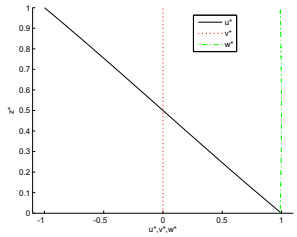

(e) Mode I - (3,0) - 3D

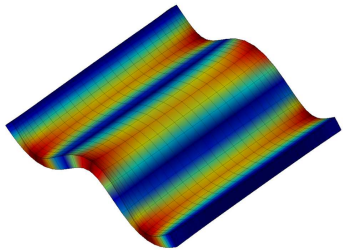

(f) Mode I - (3,0) - 2D

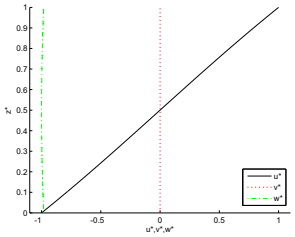

(g) Mode I - (4,0) - 3D

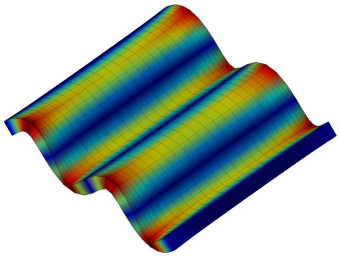

(h) Mode I - (4,0) - 2D

Figure 3: First four cylindrical bending vibration modes for the a/h=20 isotropic one-layered plate. 3D modes vs. 2D modes.

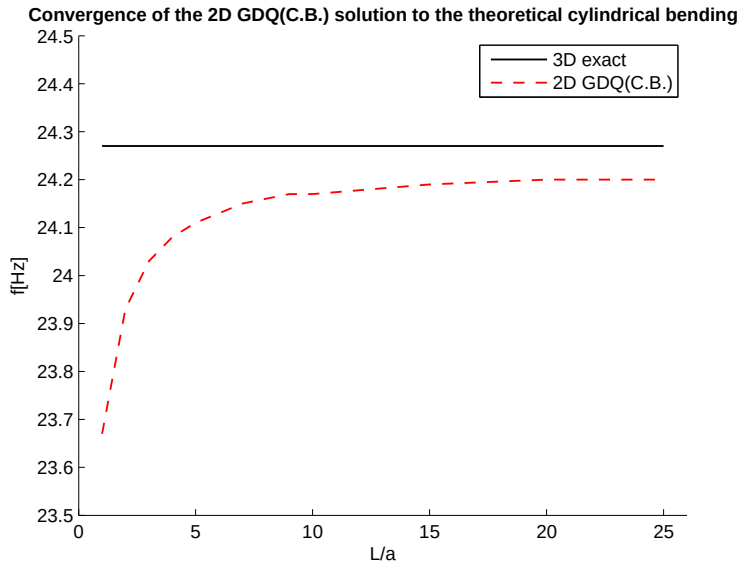

Figure 4: First mode for the a/h=100 isotropic plate: convergence of the 2D GDQ(C.B.) solution increasing the length of the simply supported edges.

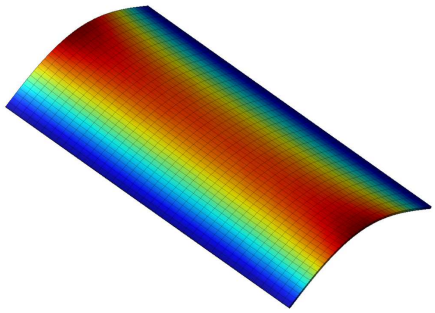

(a) L/a=2

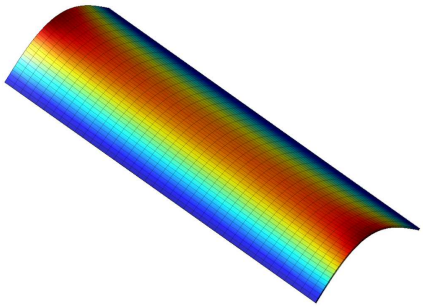

(b) L/a=3

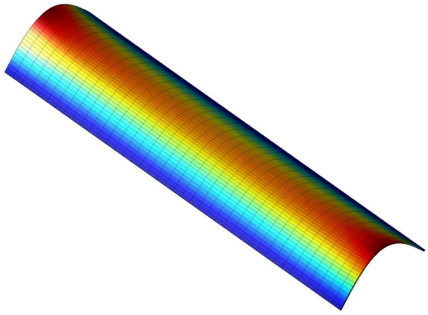

(c) L/a=4

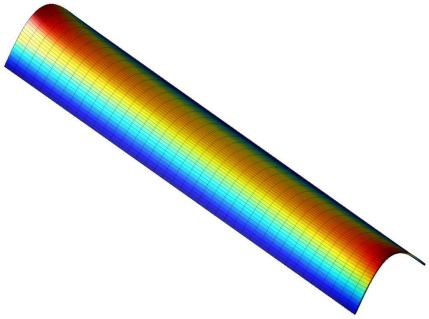

(d) L/a=5

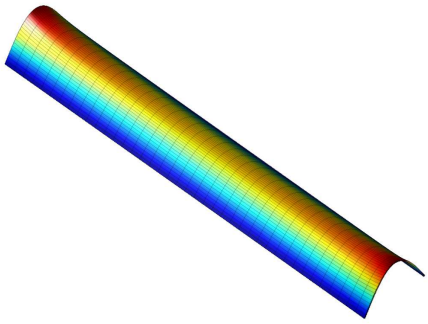

(e) L/a=6

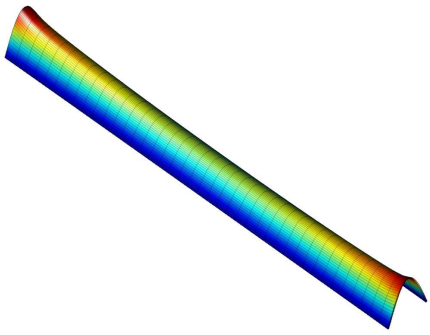

(f) L/a=10

Figure 5: First vibration mode for the a/h=100 isotropic plate: 2D GDQ(C.B.) solution and edge effects vs. length of simply supported edges.